Characterization of ambient volatile organic compounds, source apportionment, and the ozone-NOx-VOC sensitivities in a heavily polluted megacity of central China: Effect of sporting events and the emission reductions

Shijie Yu[a,b,1], Fangcheng Su[a,b,1], Shasha Yin[b,c], Shenbo Wang[b,c], Ruixin Xu[b,c], Bing He[d], Xiangge Fan[d], Minghao Yuan[d], Ruiqin Zhang[b,c]*

a. College of Chemistry, Zhengzhou University, Zhengzhou 450001, China

b. Institute of Environmental Sciences, Zhengzhou University, Zhengzhou 450001, China

c. School of Ecology and Environment, Zhengzhou University, Zhengzhou, 450001, China

d. Environmental Protection Monitoring Center Station of Zhengzhou, Zhengzhou 450007, China

*Correspondence author. Research Institute of Environmental Science, College of Environment and Ecology, Zhengzhou University High-tech Development Zone, Zhengzhou, Henan, PR China, 450001

E-mail address: rqzhang@zzu.edu.cn

[1] These authors contributed equally to this work.

Abstract: The implementation of strict emission control during the 11th National Minority Games (NMG) in September 2019 provided a valuable opportunity to assess the impact of such emission controls on the characteristics of VOCs and other air pollutants. Here, we investigated the characteristics of VOCs and the O_3-NOx-VOCs sensitivity comprehensively in Zhengzhou before, during, and after the NMG by delivering field measurements combined with the WRF (Weather Research and Forecasting)-CMAQ (Community Multi-scale Air Quality) model simulations. The average mixing ratios of VOCs during the control periods were 121±55 μg/m^3, and cut down by about 19% and 11% before and after emission reduction. The ozone precursors (NOx) also decreased significantly during the control period; however, the ozone pollution was severe during the entire observation period. Positive Matrix Factorization analysis indicated seven major sources of ambient VOCs, including coal combustion, biomass burning, vehicle exhausts, industrial processes, biogenic emissions, solvent utilization and liquefied petroleum gas (LPG). The results show that the major source emissions, such as coal combustion and solvent utilization, were significantly reduced during the control period. As for ozone formation potential (OFP), the value during the control period was 183±115 μg/m^3, which was 0.23 and 0.17 times lower than those before and after control period, respectively. Solvent utilization and combustion controls were the most important measures taken to reduce OFP during NMG period. Through control policies, it can effectively reduce carcinogenic risk. However, non-cancer risks of ambient VOC exposures were all exceeding the safe level (hazard quotient = 1) during the sampling periods, and

emphasis on the reduction of acrolein emissions was needed. In addition, the WRF/CMAQ model simulation indicated that O_3 formation was controlled by VOCs in Zhengzhou. The results of the Empirical Kinetic Modelling Approach showed that the NOx reduction in Zhengzhou might led to higher ozone pollution. It is suggested that reduction ratios of the precursors (VOCs:NOx) is more than 2, which can effectively alleviate ozone pollution.

Keywords: Volatile organic compounds; the National Minority Games; Emission control; Empirical Kinetic Modeling Approach (EKMA); Health risk assessment.

1. Introduction

Volatile organic compounds (VOCs), important precursors for the generation of near-surface ozone (O_3) and secondary organic aerosols (SOA), have received widespread attention in the world (Baudic et al., 2016; Sahu et al., 2017; Xiong and Du, 2020; Yadav et al., 2019; Yang et al., 2019a; Zeng et al., 2018; Zhang et al., 2015). Moreover, some VOCs have adverse impacts on human health, which induce cancer directly and associatewith increased long-term health risks (Hu et al., 2018; Jaars et al., 2018). Since the beginning of the 21st Century, heavy air pollution event has frequently occurred in China, characterized by regional and complex air pollution (Li et al., 2019d; Ma et al., 2019). Therefore, the improvement of air quality has become a hot issue, especially for large-scale activities held in megacities, and how to ensure air quality becomes the key to the success of the activities.

Air quality assurance refers to the systematic emission reduction and control measures of pollution sources to ensure air quality during special activities. Temporarily enhanced control measures could provide a scenario to analyze the response relationship between emission sources of pollutants and ambient air quality. Many scholars have carried out researches on pollutant characteristics and their source apportionment under different control measures for a variety of special activities. Those studies included the 2008 Beijing Olympic Games (Schleicher et al., 2012; Wang et al., 2009), the 2010 World Expo in Shanghai (Chan et al., 2015; Wang et al., 2014), the 2014 Asia-Pacific Economic Cooperation Summit in Beijing (Li et

al., 2015, 2017), 70th China Victory Day Parade anniversary (Huang et al., 2018; Ren et al., 2019) and the G20 summit in Hangzhou (Li et al., 2019b; Zhang et al., 2020). These studies all suggested that enhanced emission-reduction strategies had significant effects on improving air quality. O_3 pollution might not be improved and even worsen during the control period (Xu et al., 2019). The relationship between O_3 and its precursors is nonlinear, and unreasonable reduction of O_3 precursors might not necessarily alleviate O_3 pollution. Hence, it is necessary to investigate an in-depth understanding of the mechanism involved in O_3 formation, especially under the emission reduction scenario. However, studies on these special events have mostly focused on particulate matter and its components, and to a much lesser degree on ozone and VOCs. In particular, the discussion on O_3 sensitivity and implications for control strategies through the combination of model and observation-based methods is still lacking. Furthermore, these studies mainly focused on few metropolises in China, especially in the three most developed regions, Beijing-Tianjin-Hebei (BTH) region, Yangtze River Delta (YRD) region and Pearl River Delta (PRD) region.

From 8^{th} -16^{th} September , 2019, the 11th National Minority Games (NMG) was held in Zhengzhou, China. As the host city, Zhengzhou took emergency pollution control measures in the city and neighboring regions from 26^{th} August to 18^{th} September for enhancing air quality during NMG period. Considering that the ozone pollution is the main pollution in the region in September (Yu et al., 2020), Zhengzhou municipal government has focused on the emission reduction of VOCs and NO_x to alleviate O_3 pollution. Based on the bottom-up emission inventories and

observation-based source apportionment, major anthropogenic sources of VOCs in the area include vehicular exhaust, liquefied petroleum gas (LPG) evaporation, solvent usage and industrial emissions (Bai et al., 2020; Li et al., 2019a). Thus, they are the target emission sources when temporary invention measures are adopted for controlling air pollution during NMG period. A detailed description of the control measures is shown in Table S1. It is an excellent opportunity to determine the effects of emission control policies by using the real atmosphere as a natural laboratory. Therefore, it is necessary to investigate VOC characteristics and sources, as well as their effects on ozone production before, during, and after the control period.

This study measured 106 VOC species using on-line gas chromatography-mass spectrometry/flame ionization detector (GC-MS/FID). Meanwhile, the Weather Research and Forecasting/Community Multi-scale Air Quality (WRF/CMAQ) models were used to investigate the nonlinearity of O_3 response to precursor reductions. The main objectives of this study are to: (1) analyze the effects of emergent emission-reduction strategies on the VOC characteristics; (2) identify the crucial sources of VOCs in Zhengzhou and their changes during the NMG period; (3) investigate the contribution to ozone formation and risk assessment under control measures; and (4) assess the O_3-NO_x-VOCs sensitivity and propose control strategies for ozone episodes.

2. Methodology

2.1 Site description and chemical analysis

The sampling site is located on the rooftop of a four-story building at the municipal environmental monitoring station (MEM; 113.61° E, 34.75° N), about 6.6 km away from the Zhengzhou Olympic Sports Center (Fig. S1). The surrounding area of the sampling site is mainly commercial and residential district, and the station is 300 m west to the Qinling Road and 200 m south to the Zhongyuan Road. No significant industrial sources present around the sampling sites. The above two roads carry very heavy traffic. Accordingly, mobile source may contribute more to the VOC concentrations of the site.

VOC samples were collected from 6th August to 30th September, 2019, and divided into three periods, including pre-NMG period (6th-25th August), NMG period (26th August to 18th September) and after NMG (19th-30th September). By comparing the characteristics of VOC pollution during the three periods, the effects of control policies by government can clearly be identified and assessed.

It should be pointed out that the MEM station is located in the air monitoring network operated by Zhengzhou environmental monitoring center. The meteorological parameters (temperature, relative humidity, atmospheric pressure, wind direction and wind speed) and trace gases (O_3, NO and NO_x) were observed at the sampling site simultaneously. Information detailing relevant equipment was described by Li et al. (2019a)

Ambient VOCs were collected and analyzed continuously by using an online GC-MS/FID, and the time resolution is 1h (TH-PKU 300B, Wuhan Tianhong Instrument Co. China). This measurement was described by Li et al. (2018). Briefly, this system has two gas channels and dual detectors, in which the C_2–C_5 non-methane hydrocarbons (NMHCs) were separated on a PLOT-Al_2O_3 column (15 m × 0.32 mm × 6.0 μm, Dikma Technologies, Beijing, China) and quantified by FID, while the other species were separated on a DB-624 column (60 m × 0.25 mm × 1.4 μm, Agilent Technologies, Santa Clara, CA, USA) and detected by a mass selective detector with Deans switch.

To ensure the validity and reliability of observation data, these chemical analyses were subjected to quality assurance and quality control procedures. We used external and internal standard methods to quantify the C_2–C_5 and C_5–C_{12} compounds respectively. Before monitoring, the standard curves of five concentrations (0.4–8 ppbv) were made by using PAMS (photochemical assessment monitoring stations) standard gas, TO-15 Calibration Standards (US EPA, 1999) and four internal standard ， including bromochloromethane, 1,4-diflfluorobenzene, chlorobenzene-d5, and bromoflfluorobenzene. The above standard gases and internal standard gases were provided by Apel–Riemer Environmental, USA. In addition, we input 4 ppbv PAMS+TO-15 standard gas at 0:00 local standard time (LST) every day to calibrate the data and check the stability. The coefficients of determination (R^2) of calibration curves were mostly above 0.99 and the method detection limit (MDL) ranged from 0.004 to 0.36 μg/m^3 for each species. A total of 106 VOC species were detected,

including alkanes (29), alkenes (11), aromatics (17), halocarbons (35), Oxygenated VOCs (OVOCs) (12), acetylene, and carbon disulfide (Table S2).

2.2 WRF-CMAQ model

The WRF-CMAQ modeling system was applied to simulate ozone concentration and investigate O_3 sensitivity in this study. The modeling system, has been widely used for regional-scale air quality studies (Byun et al., 1999; Chemel et al.,2014), and more details can be found at http://cmascenter.org/cmaq/.

In this paper, the simulation period was 00:00 LST, August 5, 2019, to 23:00 LST, September 30, 2019, which corresponded to the NMG sampling periods. To eliminate the impact of the initial conditions, a 5-day spin-up period was set in the simulation. We applied four-nested domain with a grid resolution of 36 × 36 km, 12 × 12 km, 4 km × 4 km and 1 km × 1 km, respectively (as shown in Fig. S2). The gridded anthropogenic emission inventory by Tsinghua University was applied in CMAQ, and the local emission inventory of Henan Province was also input into the model (Bai et al., 2020). These modeling systems have been successfully used in previous simulations by Zhang et al. (2014) and Wang et al. (2019a). The results of WRF-CMAQ model evaluation in Zhangzhou were reported in our previous studies (Su et al., 2021).

The CMAQ developed by USEPA was used to simulate the ozone pollution processes in Zhengzhou in August and September 2019. The sensitivity of emission

sources to ozone pollution in Zhengzhou was analyzed by using source sensitivity identification tool DDM-3d (Hakami et al., 2004).

2.3 Source apportionment by PMF model

PMF analysis of VOCs was performed with the USEPA PMF 5.0 program; this receptor model is widely used for source analysis. Detailed information about this method is described in the user manual and related literature (Norris et al., 2014; Xiong and Du, 2020; Yenisoy-Karakas et al., 2020).

It must be said that not all of the VOC species were used in the PMF analysis. According to previous studies, the principles for VOC species choice were listed as following (Hui et al., 2019): (1) Species with more than 25% data missing or that fell below the MDLs were rejected; (2) Species with signal-to-noise ratio lower than 1.5 were excluded.; and (3) species with represented source tracers of emission sources were retained. Eventually, a total of 42 VOC species were selected for the source apportionment analysis. In this study, a seven-factor solution was chosen in the PMF analysis based on two parameters (Ulbrichetal.,2009): (1) Qtrue/Qrobust values and (2) Qtrue/Qtheoretical values (Fig. S3).

2.4 Potential source contribution function (PSCF)

The Potential Source Contribution Function (PSCF) is a function with conditional probability for calculating backward trajectories and identifying potential source regions. The detailed descriptions of this method were described by Bressi et al. (2014) and Waked et al. (2014). Briefly, PSCF analysis is normally used to identify

possible source areas of pollutants, such as ozone, NO_x and VOCs. PSCF calculates the probability that a source is located at latitude i and longitude j as:

$$PSCF_{ij} = \frac{m_{ij}}{n_{ij}} \quad (1)$$

Where n_{ij} is the number of times that the trajectories passed through the cell (i, j) and m_{ij} is the number of times that a source concentration was high when the trajectories passed through the cell (i, j) (Song et al., 2019a). In order to reduce the uncertainty caused by decreasing small n_{ij} value, a W_{ij} function was used in this study as calculated by Eq. (2):

$$W_{ij} = \begin{cases} 1.0, 3n_{ave} < n_{ij} \\ 0.7, 1.5n_{ave} < n_{ij} \leq 3n_{ave} \\ 0.4, 1.0n_{ave} < n_{ij} \leq 1.5n_{ave} \\ 0.2, n_{ij} \leq n_{ave} \end{cases} \quad (2)$$

In this study, the PSCF model were calculated by applying the TrajStat plugins on MeteInfoMap software version 1.4.4. The 48-h backward trajectories arriving at Zhengzhou with a trajectory height of 200 m were calculated every hour (00:00–23:00 local time). The studied domain was in the range of 15° to 65° N and 85° to 145° E in a grid of 0.1° × 0.1° cells, which contains almost all regions overlaid with entire airflow transport pathways.

2.5 Calculation of O_3 formation potential

To understand the impact of the VOC species on ozone formation, Ozone formation potential (OFP) was used, by using the following equation (Carter, 2010a):

$$OFP_i = [VOC]_i \times MIR_i \quad (3)$$

Where $[VOC]_i$ is the mass concentration of each VOC, with units of mg/m^3, MIR means maximum incremental reactivity (g O_3/g VOC), and the MIR value of each VOC is obtained from Carter (1994).

2.6 Health risk assessment

The risk assessment derived from the guidelines proposed by USEPA (2009) was used to evaluate the adverse health effects of each identified VOC in ambient air to human health, and evaluate the impact of emission reduction on health risks. In this paper, the carcinogenic and non-carcinogenic risks were calculated to assess the impacts of VOCs on human health, by using the Eqs. (4)-(7).

$$Risk = IUR \times EC \quad (4)$$

$$EC = (CA \times ET \times EF \times ED)/AT \quad (5)$$

$$HQ = EC/(RfC \times 1000) \quad (6)$$

$$HI = \sum HQ_i \quad (7)$$

Where IUR is the estimated unit risk value ($m^3/\mu g$); EC is the exposure concentration ($\mu g/m^3$); CA is the environmental concentration ($\mu g/m^3$); ET is the exposure time (h/d); EF is the exposure frequency (d/y); ED is the exposure time (y); AT is the average time (h); RfC is the reference concentration (mg/m^3); and HQ is the non-cancer inhalation hazard quotient and HI is the hazard index. Risk probability values, including RfC and IUR, were obtained through the risk model calculator established by the University of Tennessee (RAIS, 2016) and are listed in Table S3.

Out of all measured species in this paper, only 46 VOC species with known toxicity values were considered, including 44 noncarcinogenic species and 21 carcinogenic species. Target VOCs and associated toxicity values of health risk assessment are presented in the Supplementary Materials (Table S4).

3. Results and discussion

3.1 Overall observations

3.1.1 Characteristics of O_3 and other pollution gases

Fig. 1 shows the temporal trends of the O_3 and other pollutant mixing ratios during the sampling period. During the pre-NMG period, the highest O_3 hourly concentration was 252 μg/m^3 in 15:00 LST on August 23, meanwhile the max 8-h O_3 value also appeared on this day (219 μg/m^3). In addition, max 8-h O_3 concentrations presented in a total of 7 days, exceeding the ambient air quality standard (GB 3095-2012) Grade II standard of 160 μg/m^3. At this stage, the ozone pollution cause concern as the days exceeding the standard accounted for 50%. The highest hourly concentration of VOCs and NOx were 1017 and 357 μg/m^3, with a mean concentration of 150±93 and 49±46 μg/m^3 respectively. Higher O_3 precursor concentrations were observed, which maybe an important factor leading to serious photochemistry pollution.

During the control period, the O_3 precursor concentrations showed a decreasing trend, with a mean concentration of 121±55 μg/m^3 VOCs and 39±26 μg/m^3 NOx. However, the ozone pollution has not been dramatically alleviated; and mild and

moderate O_3 pollution levels accounted for 52% and 10% respectively during the NMG period according to GB 3095-2012. The phenomenon has been reported that photochemistry is still severe under emergency emission-reduction strategies (Li et al., 2019b). Due to the highly nonlinear relationships between ozone and its precursors, it is not straightforward to mitigate ozone pollution by reducing the emissions of VOCs and NOx (Tan et al., 2018; Wang et al., 2019c). A special phenomenon needs to be pointed out that the ozone concentration during the evening peak is much higher than that in the pre-NMG period. The weak titrate effect may be the main reason for the phenomena above (Chi et al., 2018; Zou et al., 2019). At the end of control, the concentration of precursors increased rapidly, and NOx concentration increased by nearly 1.6 times compared with the control stage. At the same time, the ozone pollution was still severe, the proportions of mild and moderate pollution days were 83% and 8%, respectively.

On the whole, the concentration of ozone precursors decreased during the control period (as shown in Fig.S4), and the ozone pollution was severe during the entire observation period. It should be noted that the maximum value of max 8-h O_3 concentrations in the NMG period is high of 235 $\mu g/m^3$.

3.1.2 Meteorological conditions

Meteorological conditions can significantly influence pollutant concentrations, which makes it difficult to evaluate the emission reduction brought by emission control. In this paper, the meteorological data throughout the three periods in

Zhengzhou were compared, including temperature (T), precipitation, relative humidity (RH), wind speed (WS) and visibility. As shown in Table S5, the meteorological parameters rarely changed during the three periods (T, 27.4±1.2, 24.2±3.3, and 22.3±1.5℃ for pro-, during, and post-control periods respectively; visibility, 16.7±5.5, 14.1±7.0 and 13.0±2.7 km; WS, 1.7±0.3, 1.7±0.4, and 1.5±0.3 m/s). However, the precipitation during pre-control period (236.9 mm) was much higher than those during control (39.8 mm) and post-control periods (1.6 mm). In addition, the RH in first stage is higher, which is beneficial to the air pollutants dissolving in water vapor, condensation and settlement, and then reducing the concentration of pollutants.

Meteorological conditions can influence the transmission and circulation of regional air pollutants (Ren et al., 2019). In this paper, the air clusters were analyzed by using the Hybrid Single Particle Lagrangian Integrated Trajectory model to distinguish the differences of potential source contributions in the three periods. In previous studies, regional transport has an important influence on Zhengzhou's air quality, especially the air mass from the BTH region (Jiang et al., 2019; Wang et al., 2019b). Fig. S4 shows the 48-h backward trajectories results during the sampling period. The dominant trajectory was from the east or southeast of Zhengzhou in the three periods. For the pre- and post-NMG periods, Zhengzhou is greatly affected by the air mass from BTH region, where contained high concentrations of air pollutants from anthropogenic emissions. Based on the PSCF results in Fig. 2, the high PSCF values for pollutants (including O_3, NO_2 and VOCs) were distributed significantly at

the southeast of Zhengzhou and near the Zhengzhou area. Therefore, the potential source regions for pollutants during the sampling period were mainly from the southeast of Zhengzhouand local sources within the city. For the record, high PSCF values also presented within northern Hebei Province during the pre-NMG period, where the region is the major industrialized areas in the BTH. To summarize, in addition to air pollution control measures, changes of meteorological conditions may contribute to the improvement of air quality during the NMG period.

3.2 Characteristic of VOCs during the three periods

3.2.1 Mixing ratios and chemical speciation

As illustrated in Fig. 1, the mixing ratios of hourly total VOCs (TVOCs) show average value of 150±93 μg/m^3, ranging from 41 to 1017 μg/m^3, before the control period. During control, this was reduced to average of 121±55 μg/m^3, with the range from 37 to 333 μg/m^3. After the control period, the averaged VOC concentration increased to 136±60 μg/m^3. Overall, it is clear that the emission control policies were beneficial to reduce VOC concentration, and reduced by about 19% and 11% before and after emission reduction.

The percentage distributions of VOC groups were similar in the three sampling periods (Fig. S6). Alkanes were the dominant group, accounting 37, 35, and 33% of the total VOC concentration for three periods respectively, followed by halocarbons. Notably, OVOCs slightly decreased in the entire sampling period, comprising 17, 16, and 15%, respectively. However, the active components of aromatics increased over

time. In addition to the impact of emission sources, meteorological conditions and transport might be key factors that can influence VOC compositions (Su et al., 2021).

The top 20 VOC species are summarized in Table 1. The top 20 substances were similar in the three stages, but the concentration levels were quite different. Tracers of solvent sources including hexane and dichloromethane (Huang and Hsieh, 2019; Wei et al., 2019) decreased in the control period, chopped by 42% and 47%respectively. The reduction of vinyl acetate and tetrachloroethylene is relatively large, which may be attributed to industrial emission reduction (Hsu et al., 2018; Zhang et al., 2015). In addition, the concentration of acetylene is reduced by 55% compared with the pre-NMG period, as a potential result of the control of combustion sources (Liu et al., 2020; Wu et al., 2016a).

3.2.2 Diurnal variations of ambient VOCs

The mean diurnal variations of TVOC and their compounds before, during, and after the control period are shown in Fig. S7. Clearly, the diurnal variations of TVOCs during the three periods are similar , showing higher values from evening till morning rush hours while lowest in the afternoon. The composition of alkanes, alkenes, alkynes and aromatics shows similar daily variations. Previous studies have suggested that VOCs can be oxidized by O_3, OH radicals and NO_3 radicals (Carter, 2010b). In short, the reactions with O_3 and OH radicals are the most important chemical reactions during daytime, and the reactions with NO_3 radicals and O_3 are dominant reactions for VOCs occurring at night (Atkinson and Arey, 2003). However, the

reaction rate of the OH radical is much higher than that of the NO_3 radical, and thus, the concentration of TVOC and its compounds at night is generally higher than that during the daytime (Atkinson and Arey, 2003). It should be noted that the average VOC mixing ratio at midnight during the control period was significantly lower than that in other two period, especially the concentrations of aromatics compounds were significantly decreased.

As each source type has its own fingerprint, the mean diurnal variations of tracers during the three periods are presented in Fig. 3. *I/n* -pentanes at the three periods have several minor peaks (e.g., 02:00 and 18:30 LST). The 02:00 LST peak is mainly from the freight trucks and the 7:00 LST peak is most likely from traffic rush-hour emissions (Gentner et al., 2009; Li et al., 2019c; Zheng, et al. 2018). It should be noted that during the control period, the nighttime concentration significantly decreased while the daytime concentrations of the three stages are close . Toluene, ethylbenzene, and xylenes (Fig. 3) as well as the tracer gas of NO and NO_2 (Fig. S8) at the three periods had similar diurnal patterns to those of pentane. All of the species mentioned above are tracers of traffic emission (Brito et al., 2015; Dorter, et al. 2020; Yenisoy-Karakas, et al. 2020). It is speculated that the control effect on muck truck is significant during the control period. As shown in Fig. 3, tracers of solvent utilization, such as hexane, dichloromethane, had different diurnal patterns to those of vehicle source. During the pre-NMG period, the solvent tracer emissions are so strong that they almost offset the daytime valley caused by photochemical reaction and boundary layer height (Li et al., 2019c). The daytime

levels of the NMG period are lower than those of first stage, which might attribute to the intensive control over the use of outdoor solvents. Chloromethane and acetylene are tracers of biomass burning and combustion, respectively (Mcroberts et al., 2015; Schauer et al., 2001). During control period, acetylene decreased significantly, while chloromethane remained higher levels.

3.3 Source attribution and apportionment

3.3.1 Ratios of specific compounds

During the sampling period, the great changes in the mixing ratios of VOCs may be caused by the altered contribution of emission sources. Ratios of specific VOCs has commonly been used to identify emission sources.

Because *i*- and *n*-pentane have similar atmospheric lifetimes, these *i/n* ratios are widely used to examine the impact of vehicle emissions to combustion emissions and the values varied according to sources (i.e., 0.56-0.80 for coal combustion, 1.5-3.0 for liquid gasoline, 2.2-3.8 for vehicle emissions (Yan et al., 2017; Zheng et al., 2018). Isopentane and *n*-pentane showed highly significant correlations during the three periods ($R^2 > 0.6$), suggesting the source of these two species was similar (Fig. S9). In this study, the ratios of *i/n*-pentane during the three periods were 1.5, 1.7 and 1.5, indicating that the VOCs originated from the mixed sources of coal combustion and vehicle emissions.

The toluene/benzene (T/B) ratio has also been widely applied to be indicator of sources. A previous study reported that these two species are most probably from

biomass burning, coal combustion, vehicle emissions and solvent used, when the T/B ratios ranging between 0.2-0.6, 0.6-1.0, 1.0-2.0 and > 4, respectively (Hui et al., 2018; Kumar et al., 2018; Song et al., 2019b). As shown in Fig. S9, low correlations (R^2 = 0.3-0.5) were found during the three period, suggesting a more complex set of sources for the two species. The T/B ratio among the three period was 0.78, 0.75 and 0.92, respectively, indicating that the VOCs were greatly influenced by the mixed source of coal combustion and vehicle emissions. The ratio was lower in the control period. Acetylene concentration was low but the chloromethane concentration was high during the control period, indicating biomass burning had a greater impact during the period.

3.3.2 Identification of PMF factors

The 42 most abundant species, accounted for almost 90% total VOC concentrations， were selected to apply in the PMF receptor model to analyze the relative contribution of each potential source. The factor profiles of seven emission sources, namely, liquefied petroleum gas (LPG) evaporation, industrial processes, vehicle exhausts, biomass burning, biogenic source, solvent usage and coal combustion, were identified in Fig. 4.

Source 1 was characterized by both high proportions and high abundances of ethane (38%), ethene (53%), propane (43%) and other C_3-C_5 alkanes. A high proportion of short linear alkanes, such as ethane and propane, was likely released from the use of LPG (Yadav et al., 2019; Zhang et al., 2015). Consequently factor 1

411 was assigned to LPG.

412 Source 2 accounts for larger percentages of carbon disulfide and
413 halohydrocarbon, such as *cis*-1,2-dichloroethylene, chlorotrifluoromethane,
414 trichloromethane, dichloromethane, 1,2-dichloroethane, 1,2-dichloropropane,
415 followed by some aromatics. Some previous study indicated that these species were
416 related to industrial process (Hui et al., 2020; Zhang et al., 2018). Furthermore,
417 ethylene, considered as the blood of the development in industry (Song et al., 2019a;
418 Zheng et al., 2020), accounted of almost 65% of the TVOCs in this factor. Therefore,
419 this source is considered to be related to industrial processes.

420 Source 3 was characterized by a high percentage of some C_4-C_5 alkanes and
421 aromatics. Toluene, ethyl-benzene, *m,p*-xylene, *o*-xylene, *i,n*-butane and *i,n*-pentane
422 are all associated with vehicle exhausts (Huang and Hsieh, 2019; Liu et al., 2019).
423 Furthermore, the T/B ratio was approximate 1.6, suggesting that this source was
424 significantly affected by vehicle exhaust emissions. Factor 3 also includes high
425 proportions of methyl tert-butyl ether, which is a common gasoline additive in China
426 (Yang et al., 2018). Therefore, this factor can be labeled as vehicle exhaust.

427 Source 4 has high concentrations of chloromethane, which is a typical tracer of
428 biomass burning (Ling et al., 2011; Zhang et al., 2019). The percentages of benzene
429 and toluene were lower, but they could still not be neglected, and the T/B ratio was <
430 0.5 (Li et al., 2019a). Thus, source 4 was identified as biomass burning.

431 Source 5 accounts for larger percentages of isoprene, accounting for 86% of the

TVOCs in the source. Isoprene is an indicator of biogenic emissions and emits from many plants (Guenther et al., 1995 and 1997). This factor also included a considerable proportion of intermediate products (Liu et al., 2019), such as acetone, 2-hexanone and 2-butanone. Therefore, this source is considered to be biogenic emissions.

Source 6 was differentiated by C_6-C_8 alkanes, such as *n*-hexane, methyl cyclopentane, 3-methylpentane, 2-methylpentane and 2,3-dimethylbutane. The percentages of ethyl acetate, tetrachloroethylene, carbon tetrachloride, chloroform, dichloromethane were high. Those substances are important organic solvents, and typical tracers of solvent usage (Hui et al., 2018, 2020). Meanwhile, there are virtually no other short chain hydrocarbon in this source. Therefore, source 6 was primarily attributed to solvent usage rather than industrial processes or vehicle emission source.

Source 7 was dominated by acetylene, which accounted for 75% of the TVOCs in the source. Acetylene is a typical tracer of combustion emission (Hui et al., 2019; Wu et al., 2016b). Some of the VOC species, such as alkanes and benzene, are the main components in emissions from coal burning (Liu et al., 2019; Song et al., 2019b., Yang et al., 2018). Thus, factor 7 was assigned to combustion emission.

3.3.3 Contributions of VOC sources

The concentrations of hourly mixing ratio and the relative contributions of each VOC sources are illustrated in Fig. 5 and Fig. S10. Compared with the non-control periods, the contributions of coal combustion, vehicle exhausts and solvent utilization are significantly reduced during the control period.

Conversely, the mixing ratios of LPG showed higher values during the control period. Peak values of biomass combustion presented frequently during the second period, and biomass combustion accounts for a relatively high proportion in this stage. The highest concentration was observed in the afternoon of the 18th of September. Zhengzhou and its surrounding areas are in the harvest period of crops in September, so the emissions of biomass combustion need to be concerned. Fig. S11 shows the hotspots diagram of Zhengzhou and its surrounding areas during the observation period, and the number of fire spots in September was significantly higher than that in August.

Time series of each identified source contributions are shown in Fig. 6. During the first period, solvent utilization (33 μg/m^3) was the largest contributor and accounted for 30% of TVOCs , followed by industrial process (26 μg/m^3, 23%) and vehicle exhausts (24 μg/m^3, 21%). Although it was not the heating time, coal combustion still accounted 10% of the TVOCs, probably due to several coal-fired power plants around Zhengzhou (Li et al., 2019a). In contrast, the proportion of biomass combustion was very low during this period, accounting for only 2% of the TVOCs.

During the control period, solvent utilization made the largest contribution (23%) to atmospheric VOCs, with the concentration of 23 μg/m^3, followed by and industrial process (22%), vehicle emissions (22%) and LPG (11%). Biomass burning should not be ignored in this period, accounting for 10% of total VOCs. The contribution from coal combustion was relatively low (3.5 μg/m^3), accounting only for 4% of TVOCs.

For the third period, the largest contributor was fuel combustion related to vehicle exhausts, with 30 μg/m^3, accounting for 28% of total VOCs. Industrial processes (23 μg/m^3), solvent utilization (20 μg/m^3), biomass burning (12 μg/m^3), coal combustion (11 μg/m^3), LPG (5.7 μg/m^3) and biogenic emissions (5.6 μg/m^3) accounting for 21, 19, 11, 10, 5 and 5% of total VOCs, respectively.

In summary, the concentrations of solvent utilization were reduced to the greatest extent during the control period, with the value of 10 μg/m^3 in the pre-NMG period, followed by coal combustion (7.1 μg/m^3), industrial processes (4.0 μg/m^3) and vehicle exhausts (2.2 μg/m^3). Reductions of solvent utilization, coal combustion, industrial processes and vehicle exhausts were responsible for 80, 57, 32 and 18% of the reductions in ambient VOCs, indicating that the control measures on solvent utilization and coal combustion were the most effective. In contrast, due to weak control on biomass burning and LPG, contributions from these sources were elevated. September is a harvest month in northern China, which means that biomass burning contributions might increase with time. Meanwhile, the peak contribution of this source occurred during the control period, because of a lack of relative control measures for LPG.

3.4 Atmospheric environmental implications

In this section, the atmospheric environmental implications of VOCs were discussed by calculating the values of risk assessment and ozone formation potential (OFP).

3.4.1 Risk assessment of individual VOC species

In addition to the impacts on ambient air quality, some VOC species are also toxic with various health impacts. In this paper, the non-carcinogenic risk (expressed by HQ) and carcinogenic risk (expressed by lifetime cancer risk, LCR) of hazardous VOC species were investigated, and the acceptable safety threshold were 1 and 1×10^{-6}, respectively (USEPA, 2009). On the whole, the HQ of almost substances is far below the safety threshold, indicating no chance of non-carcinogenic risk. However, only the HQ of acrolein (1.8) exceeded the value of 1, suggesting obvious chance of non-carcinogenic effects (Fig. 7). As for LCR, six species were above 1×10^{-6} in this study, including 1,2-dichloroethane (2.5×10^{-5}), chloroform (1.1×10^{-5}), 1,2-dibromoethane (8.1×10^{-6}), naphthalene (6.4×10^{-6}), benzene (5.2×10^{-6}) and tetrachloromethane (3.3×10^{-6}).

During the entire observation period, a total of seven VOCs may pose potential risks to the human health. Health risk assessment in Zhengzhou was compared with other cities, as shown in Table S3. Overall, the values of risk assessment in this study are evidently lower than those reported in Beijing (Gu et al., 2019) and Langfang (Yang et al., 2019a), whereas higher than the summer of 2018 in Zhengzhou (Li et al., 2020). Evaluated health risk assessment before, during, and after the control period shows cumulative LCR was 5.8×10^{-5}, 5.1×10^{-5} and 6.3×10^{-5} respectively during the three periods (Fig. S12). Control measures can reduce non-carcinogenic risk. On the other hand, values of six substances still exceed the acceptable safety threshold of LCR during the control period. As for non-carcinogenic risk assessment, the HI was

1.6, 2.1 and 2.1, respectively. Noticeably, the HQ of acrolein (1.9) during the control period was higher than the other two periods, which should be paid more attention. In summary, VOC concentrations decreased significantly during the control period, but still posed health risks to humans. Therefore, we need to focus on the targeted emission reduction of these characteristic substances to protect human health.

3.4.2 Variations of OFP

The OFP and their compositions during the three periods are shown in Fig. S13 and Table S6. The total OFP during the control period was 183±115 μg/m^3, which was 0.77 and 0.83 times lower than those before and after control period, respectively. As shown in Fig. S13, the aromatics were the dominant contributors to total OFP in all three periods, comprising 42, 50 and 56 %, respectively, followed by OVOCs, alkanes, alkenes, halohydrocarbon and acetylene. Aromatics played a key role in ozone formation, which is similar to many previous reports (Wang et al., 2013; Zou et al., 2015).

The source contributions to OFP were calculated by PMF model (Table 2). The most important source to ozone formation was traffic emissions. Industrial emissions and solvent usage were the second and third sources of photochemical ozone formation. Among them, solvent use has the greatest contribution to the OFP reduction with the emission reduction during the control period, explaining the 48 % reduction in OFP. Although combustion contributes only 10% of the total OFP, this source played an important role in the reduction in OFP, explaining the 33% to the

539 OFP reduction. At the same time, control of traffic and industry also reduced the OFP
540 during the games. Thus, solvent utilization and combustion controls were the most
541 important measures taken to reduce OFP during National Minority Games 2019 in
542 Zhengzhou. However, the current knowledge about formation mechanisms of O_3 is
543 still very limited, and the next section discuss the sensitivity of ozone.

544

545 3.5 O_3-NOx-VOCs sensitivity and control strategies

546 The impact of ozone precursors on ozone formation can be described as either a
547 NOx-limited or VOCs-limited regime, which is an important step in developing
548 effective control strategies to reduce regional ozone pollution. The ratios of
549 VOCs/NOx have been widely used to determine the ozone formation regime.
550 Generally, VOCs-sensitive regimes occur when VOCs/NOx ratios are lower than 10
551 (ppb C/ppbv); ozone formation to be NOx-limited when the ratios are greater than
552 20.(Li et al., 2019a, 2021; Sillman, 1999).

553 The diurnal variations of the VOCs/NOx ratios before, during, and after the
554 control period are shown in Fig. 8, and the ratios for the three periods showed similar
555 daily variations. Higher ratios were observed at midnight (1:00-6:00), especially
556 during the control period (Fig. 8) due to the emission reduction of NOx emissions,
557 with the VOCs/NOx ratios of 10. Afterwards, the ratio decreased rapidly, indicating
558 that NOx concentration increased faster than NMHCs due to the effect of vehicular
559 emissions (Zou et al., 2019). Thereafter, the ratio of VOC/NOx also increased with

560 the continuous accumulation of O_3 concentration.

561 At the peak time of O_3 concentration (12:00-16:00), the average VOCs/NOx
562 ratio was approximately 9.3 during the pre-NMG period, which was slightly lower
563 than 10 and thus proved that the ozone generation in this period was limited by VOCs.
564 During the control period, the ratio in the afternoon was lower than that in the
565 pre-NMG period, with a mean value of 7.1. In this study, the mean values of
566 VOCs/NOx (ppbv C/ppbv) were below 10 during all three periods, indicating that the
567 O_3 formation was sensitive to VOCs in Zhengzhou, and the reductions of the VOC
568 emissions will be beneficial for O_3 alleviation. Meanwhile, the daily variation of VOC
569 (MIR)/ NOx is similar to that of VOCs/NOx (ppbv C/ppbv).

570 It should be noted that ozone sensitivity can only be initially determined by the
571 VOCs/NOx ratio, and the next part it will be verified by WRF-CMAQ model.

572 As shown in Fig 9, the values of sensitivity_NO_X/sensitivity_VOCs were
573 generally lower than 0.8 in the urban district of Zhengzhou and its surrounding areas,
574 while the ratio of the western part of Zhengzhou is more than 1.2. Thus, O_3 formation
575 is quite sensitive to VOCs, and that means VOCs should be controlled in priority to
576 the effect control of O_3. To achieve a more effective reduction, it is necessary to study
577 reduction ratio that has the greatest effect on control strategies in reducing ozone
578 concentration.

579 The EKMA of O_3-VOC-NO_X sensitivity analysis is presented in Fig. 10. The
580 results reflect that cutting VOCs can alleviate ozone pollution, while reducing NOx

concentration might lead to the increase of ozone concentration. Some scholars have pointed out that the reaction rate constant between NOx and OH radical is 5.5 times higher than that of VOCs and OH radical (Chen et al., 2019). Therefore, the reduction of NOx may lead to increase OH radicals from the VOC oxidation cycle thereby promoting the formation of O_3. Response of ozone to its precursors (VOCs and NOx) under different emission reduction scenarios are shown in Fig. 10. Reduction of ozone precursors will not improve photochemical pollution when reduction ratios of the precursors (VOC:NOx) is less than 1. As shown in Fig. 10, O_3 levels decreased most effectively for the only VOC reduction scheme with VOCs: NOx = 2:1 (using mol ratio). It should be noted that it is nearly impossible to reduce VOC emissions only while NOx remains unchanged, because VOCs (particularly anthropogenic VOCs) and NOx are generally co-emitted (Chen et al., 2019).

During the NMG period, the government has carried out stringent emission controls. The concentrations of ozone precursors showed a decreasing trend, but the ozone pollution was still serious. Unreasonable emission reduction may be an important factor leading to ozone pollution. Combined with the results of this study, it is suggested that reduction ratios of the precursors (VOCs:NOx) should be more than 2 to effectively alleviate ozone pollution. Controlling VOC sources is the key to alleviate the local ozone pollution, especially the control of aromatic hydrocarbons. The solvent usage are non-combustion processes, and therefore reducing VOC emission from this source will not contribute to the decrease of NO_X emission. This finding could guide the formulation and implementation of effective O_3 control

603 strategies in Zhengzhou.

604

4. Conclusions

A number of strict emission control measures were implemented in Zhengzhou and its surrounding area to ensure good air quality during NMG period. The concentrations of VOCs and NO_x decreased significantly; however, O_3 pollution has not been effectively alleviated. To provide scientific references and guidance for atmospheric control strategies, this study systematically quantified the impacts of characterizing level, photochemical reactivity, source contribution of the VOCs and the ozone-NOx-VOC sensitivities during sporting events in Zhengzhou.

The mixing ratios of TVOCs during control period was 121±55 μg/m^3, and cut down by about 19% and 11% than those before and after emission reduction. Source apportioning showed that solvent usage, industrial processes, vehicle exhausts, LPG, biomass burning, biogenic source and coal combustion were the major sources of VOCs, and the seven sources accounting for 23%, 23%, 22%, 11%, 10%, 8% and 4% during the MNG period. The control measures on solvent utilization and coal combustion were most effective, accounting for 80 and 57% of the reductions in ambient VOCs, respectively. However, contributions of biomass burning were elevated. The total OFP during the control period was 183±115 μg/m^3, which was 0.23 and 0.17 times lower than those before and after control period, respectively. Measurements on solvent utilization and combustion were the most important controls to reduce OFP during NMG period.

The O_3-NOx-VOC sensitivity showed that Zhengzhou is under VOC-sensitive

626 regimes. Cutting VOCs can alleviate ozone pollution, while excessively reducing
627 NOx concentration might lead to the increase of ozone concentration. Unreasonable
628 emission reduction may aggravate ozone pollution during control periods. It is
629 suggested that emission reduction ratios of the precursors (VOC:NOx) should be
630 more than 2. Considering that the solvent usage are non-combustion processes,
631 reducing VOC emission from this sources will not cause the decrease of NO_X
632 emission, therefore the solvent source can be controlled preferentially.
633

Data availability

The data set is available to the community and can be accessed by request from Ruiqin Zhang (rqzhang@zzu.edu.cn).

Author contribution

YSJ and ZRQ planned and organized the study, and were deeply involved in writing the manuscript. SFC, YSS and WSB performed the atmospheric measurements and data analysis and wrote the manuscript. HB, FXG and YMH assisted heavily with the atmospheric measurements and data analysis. SFC and XRX conducted the model development and data analysis.

Other coauthors provided useful insights in data analysis and contributed to the writing of the manuscript.

YSJ and SFC contributed equally to this work.

Acknowledgments

This work was supported by the Study of Collaborative Control of $PM_{2.5}$ and O_3 Pollution in Zhengzhou City (No. 20200321A) and National Key Research and Development Program of China (No. 2017YFC0212403).

References

Atkinson, R., Arey, J., 2003. Atmospheric degradation of volatile organic compounds. Chem. Rev. 103, 4605–4638.

Bai, L., Lu, X., Yin, S., Zhang, H., Ma, S., Wang, C., Li, Y., Zhang, R., 2020. A recent emission inventory of multiple air pollutant, $PM_{2.5}$ chemical species and its spatial-temporal characteristics in central China. J. Clean. Prod. 269, 112-114.

Baudic, A., Gros, V., Sauvage, S., Locoge, N., Sanchez, O., Sarda-Estève, R., Kalogridis, C., Petit, J.-E., Bonnaire, N., Baisnée, D., Favez, O., Albinet, A., Sciare, J., Bonsang, B., 2016. Seasonal variability and source apportionment of volatile organic compounds (VOCs) in the Paris megacity (France). Atmos. Chem. Phys. 16, 11961-11989.

Bressi, M., Sciare, J., Ghersi, V., Mihalopoulos, N., Petit, J.E., Nicolas, J.B., Moukhtar, S., Rosso, A., Feron, A., Bonnaire, N., Poulakis, E., Theodosi, C., 2014. Sources and geographical origins of fine aerosols in Paris (France). Atmos. Chem. Phys. 14, 8813–8839.

Brito, J., Wurm, F., Serrano, A., Assuno, J., Artaxo, P., Godoy, J., Artaxo, P., 2015. Vehicular Emission Ratios of VOCs in a Megacity Impacted by Extensive Ethanol Use: Results of Ambient Measurements in Sao Paulo, Brazil. Environ. Sci. Technol. 49:11381-7.

Byun, D., Ching, J., 1999. Science Algorithms of the EPA Models-3 Community Multiscale Air Quality (CMAQ) Modeling System. US Environmental Protection Agency, Office of Research and Development, Washington, DC,

USA.

Carter, W., 1994. Development of ozone reactivity scales for volatile organic compounds. J. Air Waste Manag. Assoc. 44, 881–899.

Carter, W., 2010a. Updated maximum incremental reactivity scale and hydrocarbon bin reactivities for regulatory applications. Prep. Calif. Air Resour. Board Contract. 07-339.

Carter, W., 2010b. Development of the SAPRC-07 chemical mechanism. Atmos. Environ. 44, 5324–5335.

Chan, K.L., Hartl, A., Lam, Y.F., Xie, P.H., Liu, W.Q., Cheung, H.M., Lampel, J., Pöhler, D., Li, A., Xu, J., Zhou, H.J., Ning, Z., Wenig, M.O., 2015. Observations of tropospheric NO_2 using ground based MAX-DOAS and OMI measurements during the Shanghai World Expo 2010. Atmos. Environ. 119, 45-58.

Chen, X., Situ, S., Zhang, Q., Wang, X., Sha, C., Zhouc, L., Wu, L., Wu, L., Ye, L., Li, C., 2019. The synergetic control of NO_2 and O_3 concentrations in a manufacturing city of southern China. Atmos. Environ. 201, 402-416.

Chemel, C., Fisher, B., Kong, X., Francis, X., Sokhi, R., Good, N., Collins, W., Folberth, G., 2014. Application of chemical transport model CMAQ to policy decisions regarding PM2.5 in the UK. Atmos. Environ. 82, 410–417.

Chi, X., Liu, C., Xie, Z., Fan, G., Wang, Y., He, P., Fan, S., Hong, Q., Wang, Z., Yu, X., Yue, F., Duan, J., Zhang, P., Liu, J., 2018. Observations of ozone vertical profiles and corresponding precursors in the low troposphere in Beijing, China. Atmos. Res. 213, 224-235.

699 Drter, M., Odabasi, M., Yenisoy-Karaka, S., 2020. Source apportionment of biogenic
700 and anthropogenic VOCs in Bolu plateau. Sci. Total Environ. 731:139201.
701 Gentner, D., Harley, R., Miller, A., Goldstein, A., 2009. Diurnal and seasonal
702 variability of gasoline-related volatile organic compound emissions in Riverside,
703 California. Environ. Sci. Technol. 43, 4247–4252.
704 Guenther, A., 1997. Seasonal and spatial variations in natural volatile organic
705 compound emissions. Ecol. Appl. 7, 34–45.
706 Guenther, A., Hewitt, C.N., Erickson, D., Fall, R., Geron, C., Graedel, T., Harley, P.,
707 Klinger, L., Lerdau, M., McKay, W.A., Pierce, T., Scholes, B., Steinbrecher, R.,
708 Tallamraju, R., Taylor, J., Zimmerman, P., 1995. A global model of natural
709 volatile organic compound emissions. J. Geophys. Res. 100, 8873–8892.
710 Gu, Y., Li, Q., Wei, D., Gao, L., Tan, L., Su, G., Liu, G., Liu, W., Li, C., Wang, Q.,
711 2019. Emission characteristics of 99 NMVOCs in different seasonal days and the
712 relationship with air quality parameters in Beijing, China. Ecotoxicol. Environ.
713 Saf. 169, 797-806.
714 Hakami, A.; Henze, D. K.; Seinfeld, J. H.; Singh, K.; Sandu, A.; Kim, S.; Byun, D.;
715 Li, Q., 2007. The adjoint of CMAQ. Environ. Sci. Technol. 41, 7807-7817.
716 Hsu, C.Y., Chiang, H.C., Shie, R.H., Ku, C.H., Lin, T.Y., Chen, M.J., Chen, N.T.,
717 Chen, Y.C., 2018. Ambient VOCs in residential areas near a large-scale
718 petrochemical complex: Spatiotemporal variation, source apportionment and
719 health risk. Environ. Pollut. 240, 95-104.
720 Hu, R., Liu, G., Zhang, H., Xue, H., Wang, X., 2018. Levels, characteristics and

721 health risk assessment of VOCs in different functional zones of Hefei.
722 Ecotoxicol. Environ. Saf. 160, 301-307.
723 Huang, W., Fang, D., Shang, J., Li, Z., Zhang, Y., Huo, P., Liu, Z., Schauer, J.J.,
724 Zhang, Y., 2018. Relative impact of short-term emissions controls on gas and
725 particle-phase oxidative potential during the 2015 China Victory Day Parade in
726 Beijing, China. Atmos. Environ. 183, 49-56.
727 Huang, Y.S., Hsieh, C.C., 2019. Ambient volatile organic compound presence in the
728 highly urbanized city: source apportionment and emission position. Atmos.
729 Environ. 206, 45-59.
730 Hui, L., Liu, X., Tan, Q., Feng, M., An, J., Qu, Y., Zhang, Y., Cheng, N., 2019. VOC
731 characteristics, sources and contributions to SOA formation during haze events
732 in Wuhan, Central China. Sci. Total. Environ. 650, 2624-2639.
733 Hui, L., Liu, X., Tan, Q., Feng, M., An, J., Qu, Y., Zhang, Y., Deng, Y., Zhai, R.,
734 Wang, Z., 2020. VOC characteristics, chemical reactivity and sources in urban
735 Wuhan, central China. Atmos. Environ. 224, 117340.
736 Hui, L., Liu, X., Tan, Q., Feng, M., An, J., Qu, Y., Zhang, Y., Jiang, M., 2018.
737 Characteristics, source apportionment and contribution of VOCs to ozone
738 formation in Wuhan, Central China. Atmos. Environ. 192, 55-71.
739 Jaars, K., Vestenius, M., van Zyl, P.G., Beukes, J.P., Hellén, H., Vakkari, V., Venter,
740 M., Josipovic, M., Hakola, H., 2018. Receptor modelling and risk assessment of
741 volatile organic compounds measured at a regional background site in South
742 Africa. Atmos. Environ. 172, 133-148.

743 Jiang, N., Li, L., Wang, S., Li, Q., Dong, Z., Duan, S., Zhang, R., Li, S., 2019.
744 Variation tendency of pollution characterization, sources, and health risks of
745 $PM_{2.5}$-bound polycyclic aromatic hydrocarbons in an emerging megacity in
746 China: Based on three-year data. Atmos. Res. 217, 81-92.
747 Kumar, A., Singh, D., Kumar, K., Singh, B.B., Jain, V.K., 2018. Distribution of
748 VOCs in urban and rural atmospheres of subtropical India: Temporal variation,
749 source attribution, ratios, OFP and risk assessment. Sci. Total. Environ. 613-614,
750 492-501.
751 Li, B.W., Ho, S.S.H., Gong, S.L., Ni, J.W., Li, H.R., Han, L.Y., Yang, Y., Qi, Y.J.,
752 Zhao, D.X., 2019a. Characterization of VOCs and their related atmospheric
753 processes in a central Chinese city during severe ozone pollution periods. Atmos.
754 Chem. Phys. 19, 617-638.
755 Li, H., Wang, D., Cui, L., Gao, Y., Huo, J., Wang, X., Zhang, Z., Tan, Y., Huang, Y.,
756 Cao, J., Chow, J.C., Lee, S.C., Fu, Q., 2019b. Characteristics of atmospheric
757 $PM_{2.5}$ composition during the implementation of stringent pollution control
758 measures in shanghai for the 2016 G20 summit. Sci. Total. Environ. 648,
759 1121-1129.
760 Li, J., Xie, S.D., Zeng, L.M., Li, L.Y., Li, Y.Q., Wu, R.R., 2015. Characterization of
761 ambient volatile organic compounds and their sources in Beijing, before, during,
762 and after Asia-Pacific Economic Cooperation China 2014. Atmos. Chem. Phys.
763 15, 7945-7959.
764 Li, J., Zhai, C., Yu, J., Liu, R., Li, Y., Zeng, L., Xie, S., 2018. Spatiotemporal

765 variations of ambient volatile organic compounds and their sources in Chongqing,
766 a mountainous megacity in China. Sci. Total. Environ. 627, 1442-1452.
767 Li, K., Li, J., Tong, S., Wang, W., Huang, R.-J., Ge, M., 2019c. Characteristics of
768 wintertime VOCs in suburban and urban Beijing: concentrations, emission ratios,
769 and festival effects. Atmos. Chem. Phys. 19, 8021-8036.
770 Li, K., Li, J., Wang, W., Tong, S., Liggio, J., Ge, M., 2017. Evaluating the
771 effectiveness of joint emission control policies on the reduction of ambient
772 VOCs: Implications from observation during the 2014 APEC summit in
773 suburban Beijing. Atmos. Environ. 164, 117-127.
774 Li, R., Wang, Z., Cui, L., Fu, H., Zhang, L., Kong, L., Chen, W., Chen, J., 2019d. Air
775 pollution characteristics in China during 2015-2016: Spatiotemporal variations
776 and key meteorological factors. Sci. Total. Environ. 648, 902-915.
777 Li, Y., Yin, S., Yu, S., Bai, L., Wang, X., Lu, X., Ma, S., 2021. Characteristics of
778 ozone pollution and the sensitivity to precursors during early summer in central
779 plain, China. J. Environ. Sci. (in China). 99, 354-368.
780 Li, Y., Yin, S., Yu, S., Yuan, M., Dong, Z., Zhang, D., Yang, L., Zhang, R., 2020.
781 Characteristics, source apportionment and health risks of ambient VOCs during
782 high ozone period at an urban site in central plain, China. Chemosphere 250,
783 126283.
784 Ling, Z.H., Guo, H., Cheng, H.R., Yu, Y.F., 2011. Sources of ambient volatile
785 organic compounds and their contributions to photochemical ozone formation at
786 a site in the Pearl River Delta, southern China. Environ. Pollut. 159, 2310-2319.

787 Liu, Y., Song, M., Liu, X., Zhang, Y., Hui, L., Kong, L., Zhang, Y., Zhang, C., Qu, Y.,
788 An, J., Ma, D., Tan, Q., Feng, M., 2020. Characterization and sources of volatile
789 organic compounds (VOCs) and their related changes during ozone pollution
790 days in 2016 in Beijing, China. Environ. Pollut. 257, 113599.
791 Liu, Y., Wang, H., Jing, S., Gao, Y., Peng, Y., Lou, S., Cheng, T., Tao, S., Li, L., Li,
792 Y., Huang, D., Wang, Q., An, J., 2019. Characteristics and sources of volatile
793 organic compounds (VOCs) in Shanghai during summer: Implications of
794 regional transport. Atmos. Environ. 215, 116902.
795 Ma, T., Duan, F., He, K., Qin, Y., Tong, D., Geng, G., Liu, X., Li, H., Yang, S., Ye,
796 S., Xu, B., Zhang, Q., Ma, Y., 2019. Air pollution characteristics and their
797 relationship with emissions and meteorology in the Yangtze River Delta region
798 during 2014-2016. J. Environ. Sci. (in China). 83, 8-20.
799 Mcroberts, W., Keppler, F., Harper, D., Hamilton, J., 2015. Seasonal changes in
800 chlorine and methoxyl content of leaves of deciduous trees and their impact on
801 release of chloromethane and methanol at elevated temperatures. Environ. Chem.
802 12, 426-437.
803 Norris, G., Duvall, R., Brown, S., Bai, S., 2014. EPA Positive Matrix Factorization
804 (PMF) 5.0. Fundamentals and User Guide. US Environmental Protection Agency,
805 EPA/600/R-14/108, Washington, DC.
806 RAIS (The Risk Assessment Information System), 2009. http://rais.ornl.gov/tools/
807 profile.php.
808 Ren, Y., Li, H., Meng, F., Wang, G., Zhang, H., Yang, T., Li, W., Ji, Y., Bi, F., Wang,

X., 2019. Impact of emission controls on air quality in Beijing during the 2015 China Victory Day Parade: Implication from organic aerosols. Atmos. Environ. 198, 207-214.

Sahu, L., Tripathi, N., Yadav, R., 2017. Contribution of biogenic and photochemical sources to ambient VOCs during winter to summer transition at a semi-arid urban site in India. Environ. Pollut. 229:595-606.

Schauer, J., Kleeman, M., Cass, G., Simoneit, B., 2001. Measurement of emissions from air pollution sources. 3. C1−C29 organic compounds fromfireplace combustion of wood. Environ. Sci. Technol. 35, 1716–1728.

Schleicher, N., Norra, S., Chen, Y., 2012. Efficiency of mitigation measures to reduce particulate air pollution-a case study during the Olympic Summer Games 2008 in Beijing, China. Sci. Total. Environ. 427–428, 146-158.

Sillman, S., 1999. The relation between ozone, NOx and hydrocarbons in urban and polluted rural environments. Atmos. Environ. 33, 1821–1845.

Song, C., Liu, B., Dai, Q., Li, H., Mao, H., 2019a. Temperature dependence and source apportionment of volatile organic compounds (VOCs) at an urban site on the north China plain. Atmos. Environ. 207, 167-181.

Song, M., Liu, X., Zhang, Y., Shao, M., Lu, K., Tan, Q., Feng, M., Qu, Y., 2019b. Sources and abatement mechanisms of VOCs in southern China. Atmos. Environ. 201, 28-40.

Su, F., Xu, Q., Wang, K., Yin, S., Wang, S., Zhang, R., Tang, X., Ying, Q., 2021. On the effectiveness of short-term intensive emission controls on ozone and

831 particulate matter in a heavily polluted megacity in central China. Atmos.
832 Environ. 246, 118111.
833 Tan, Z., Lu, K., Dong, H., Hu, M., Li, X., Liu, Y., Lu, S., Shao, M., Su, R., Wang, H.,
834 Wu, Y., Wahner, A., Zhang, Y., 2018. Explicit diagnosis of the local ozone
835 production rate and the ozone-NOx-VOC sensitivities. Sci. Bull. 63, 1067-1076.
836 Ulbrich, I., Canagaratna, M., Zhang, Q., Worsnop, D., Jimenez, J., 2009.
837 Interpretation of organic components from Positive Matrix Factorization of
838 aerosol mass spectrometric data. Atmos. Chem. Phys. 9, 2891–2918.
839 USEPA, 2009. Risk Assessment Guidance for Superfund Volume I: Human Health
840 Evaluation Manual (Part F, Supplemental Guidance for Inhalation Risk
841 Assessment). EPA-540-R-070–002. US Environmental Protection Agency,
842 Washington, DC, USA.
843 Waked, A., Favez, O., Alleman, L.Y., Piot, C., Petit, J.E., Delaunay, T., Verlinden, E.,
844 Golly, B., Besombes, J.L., Jaffrezo, J.L., Leoz-Garziandia, E., 2014. Source
845 apportionment of PM_{10} in a north-western Europe regional urban background site
846 (Lens, France) using positive matrix factorization and including primary
847 biogenic emissions. Atmos. Chem. Phys. 14, 3325–3346.
848 Wang, H., Chen, C., Wang, Q., Huang, C., Su, L., Huang, H., Lou, S., Zhou, M., Li,
849 L., Qiao, L., Wang, Y., 2013. Chemical loss of volatile organic compounds and
850 its impact on the source analysis through a two-year continuous measurement.
851 Atmos. Environ. 80, 488–498.
852 Wang, M., Zhu, T., Zheng, J., Zhang, RY., Zhang, SQ., Xie, XX., 2009. Use of a

mobile laboratory to evaluate changes in on-road air pollutants during the Beijing 2008 Summer Olympics. Atmos. Chem. Phys. 9, 8247–8263.

Wang, N., Lyu, X., Deng, X., Huang, X., Jiang, F., Ding, A., 2019c. Aggravating O_3 pollution due to NOx emission control in eastern China. Sci. Total. Environ. 677, 732-744.

Wang, P., Chen, Y., Hu, J., Zhang, H., Ying, Q., 2019a. Attribution of tropospheric ozone to NOx and VOC emissions: considering ozone formation in the transition regime. Environ. Sci. Technol. 53, 1404-1412.

Wang, S., He, B., Yuan, M., Su, F., Yin, S., Yan, Q., Jiang, N., Zhang, R., Tang, X., 2019b. Characterization of individual particles and meteorological conditions during the cold season in Zhengzhou using a single particle aerosol mass spectrometer. Atmos. Res. 219, 13-23.

Wang, W., Jing, L., Zhan, J., Wang, B., Zhang, D.P., Zhang, H.W., Wang, D.Q., Yang, Y., Zhao, J., Sun, Y.F., Bi, X.H., Wang, X.T., Feng, J.L., 2014. Nitrated polycyclic aromatic hydrocarbon pollution during the Shanghai World Expo 2010. Atmos. Environ. 89, 242-248.

Wei, X.-Y., Liu, M., Yang, J., Du, W.-N., Sun, X., Huang, Y.-P., Zhang, X., Khalil, S.K., Luo, D.-M., Zhou, Y.-D., 2019. Characterization of $PM_{2.5}$-bound PAHs and carbonaceous aerosols during three-month severe haze episode in Shanghai, China: Chemical composition, source apportionment and long-range transportation. Atmos. Environ. 203, 1-9.

Wu, F., Yu, Y., Sun, J., Zhang, J., Wang, J., Tang, G., Wang, Y., 2016a.

875 Characteristics, source apportionment and reactivity of ambient volatile organic
876 compounds at Dinghu Mountain in Guangdong Province, China. Sci. Total.
877 Environ. 548-549, 347-359.
878 Wu, R., Li, J., Hao, Y., Li, Y., Zeng, L., Xie, S., 2016b. Evolution process and
879 sources of ambient volatile organic compounds during a severe haze event in
880 Beijing, China. Sci. Total. Environ. 560-561, 62-72.
881 Xiong, Y., Du, K., 2020. Source-resolved attribution of ground-level ozone formation
882 potential from VOC emissions in Metropolitan Vancouver, BC. Sci. Total.
883 Environ. 721, 137698.
884 Xu, W., Liu, X., Liu, L., Dore, A.J., Tang, A., Lu, L., Wu, Q., Zhang, Y., Hao, T., Pan,
885 Y., Chen, J., Zhang, F., 2019. Impact of emission controls on air quality in
886 Beijing during APEC 2014: Implications from water-soluble ions and
887 carbonaceous aerosol in $PM_{2.5}$ and their precursors. Atmos. Environ. 210,
888 241-252.
889 Yadav, R., Sahu, L.K., Tripathi, N., Pal, D., Beig, G., Jaaffrey, S.N.A., 2019.
890 Investigation of emission characteristics of NMVOCs over urban site of western
891 India. Environ. Pollut. 252, 245-255.
892 Yan, Y., Peng, L., Li, R., Li, Y., Li, L., Bai, H., 2017. Concentration, ozone formation
893 potential and source analysis of volatile organic compounds (VOCs) in a thermal
894 power station centralized area: A study in Shuozhou, China. Environ. Pollut. 223,
895 295-304.
896 Yang, W., Zhang, Y., Wang, X., Li, S., Zhu, M., Yu, Q., Li, G., Huang, Z., Zhang, H.,

Wu, Z., Song, W., Tan, J., Shao, M., 2018. Volatile organic compounds at a rural site in Beijing: influence of temporary emission control and wintertime heating. Atmos. Chem. Phys. 18, 12663-12682.

Yang, Y., Ji, D., Sun, J., Wang, Y., Yao, D., Zhao, S., Yu, X., Zeng, L., Zhang, R., Zhang, H., Wang, Y., Wang, Y., 2019a. Ambient volatile organic compounds in a suburban site between Beijing and Tianjin: Concentration levels, source apportionment and health risk assessment. Sci. Total. Environ. 695, 133889.

Yang, Y., Liu, X., Zheng, J., Tan, Q., Feng, M., Qu, Y., An, J., Cheng, N., 2019b. Characteristics of one-year observation of VOCs, NOx, and O_3 at an urban site in Wuhan, China. J. Environ. Sci. (in China). 79, 297-310.

Yenisoy-Karakas, S., Dorter, M., Odabasi, M., 2020. Intraday and interday variations of 69 volatile organic compounds (BVOCs and AVOCs) and their source profiles at a semi-urban site. Sci. Total. Environ. 723, 138028.

Yu, S., Yin, S., Zhang, R., Wang, L., Su, F., Zhang, Y., Yang, J., 2020. Spatiotemporal characterization and regional contributions of O_3 and NO_2: An investigation of two years of monitoring data in Henan, China. J. Environ. Sci. (in China). 90, 29-40.

Zeng, P., Lyu, X.P., Guo, H., Cheng, H.R., Jiang, F., Pan, W.Z., Wang, Z.W., Liang, S.W., Hu, Y.Q., 2018. Causes of ozone pollution in summer in Wuhan, Central China. Environ. Pollut. 241, 852-861.

Zhang, H., Chen, G., Hu, J., Chen, S., Wiedinmyer, C., Kleeman, M., Ying, Q., 2014. Evaluation of a seven-year air quality simulation using the Weather Research

and Forecasting (WRF)/Community Multiscale Air Quality (CMAQ) models in the eastern United States. Sci. Total. Environ. 473-474, 275-85.

Zhang, Y., Hong, Z., Chen, J., Xu, L., Hong, Y., Li, M., Hao, H., Chen, Y., Qiu, Y., Wu, X., Li, J.-R., Tong, L., Xiao, H., 2020. Impact of control measures and typhoon weather on characteristics and formation of $PM_{2.5}$ during the 2016 G20 summit in China. Atmos. Environ. 224, 233-248.

Zhang, Y., Li, R., Fu, H., Zhou, D., Chen, J., 2018. Observation and analysis of atmospheric volatile organic compounds in a typical petrochemical area in Yangtze River Delta, China. J. Environ. Sci. (in China). 71, 117312.

Zhang, Y., Sun, J., Zheng, P., Chen, T., Liu, Y., Han, G., Simpson, I.J., Wang, X., Blake, D.R., Li, Z., Yang, X., Qi, Y., Wang, Q., Wang, W., Xue, L., 2019. Observations of C1-C5 alkyl nitrates in the Yellow River Delta, northern China: Effects of biomass burning and oil field emissions. Sci. Total. Environ. 656, 129-139.

Zhang, Y., Wang, X., Zhang, Z., Lu, S., Huang, Z., Li, L., 2015. Sources of C(2)-C(4) alkenes, the most important ozone nonmethane hydrocarbon precursors in the Pearl River Delta region. Sci. Total. Environ. 502, 236-245.

Zheng, H., Kong, S., Xing, X., Mao, Y., Hu, T., Ding, Y., Li, G., Liu, D., Li, S., Qi, S., 2018. Monitoring of volatile organic compounds (VOCs) from an oil and gas station in northwest China for 1 year. Atmos. Chem. Phys. 18, 4567-4595.

Zheng, H., Kong, S., Yan, Y., Chen, N., Yao, L., Liu, X., Wu, F., Cheng, Y., Niu, Z., Zheng, S., Zeng, X., Yan, Q., Wu, J., Zheng, M., Liu, D., Zhao, D., Qi, S., 2020.

Compositions, sources and health risks of ambient volatile organic compounds (VOCs) at a petrochemical industrial park along the Yangtze River. Sci. Total. Environ. 703, 135505.

Zou, Y., Charlesworth, E., Yin, C.Q., Yan, X.L., Deng, X.J., Li, F., 2019. The weekday/weekend ozone differences induced by the emissions change during summer and autumn in Guangzhou, China. Atmos. Environ. 199, 114-126.

Zou, Y., Deng, X.J., Zhu, D., Gong, D.C., Wang, H., Li, F., Tan, H.B., Deng, T., Mai, B.R., Liu, X.T., Wang, B.G., 2015. Characteristics of 1 year of observational data of VOCs, NOx and O_3 at a suburban site in guangzhou, China. Atmos. Chem. Phys. 15, 6625–6636.

Figure list:

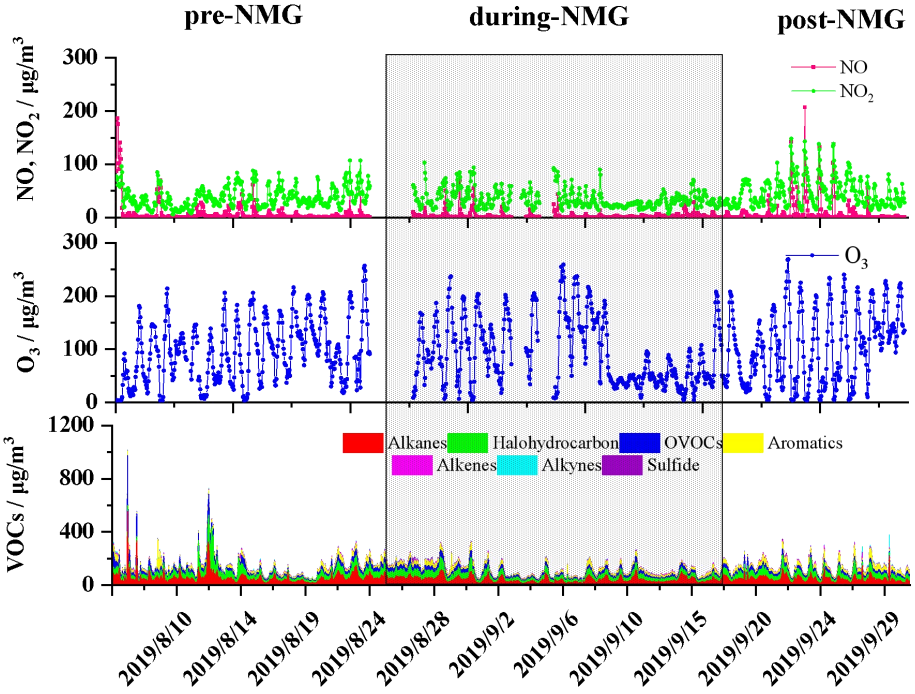

Fig. 1 Time series of VOCs and trace gases during the sampling period in Zhengzhou.

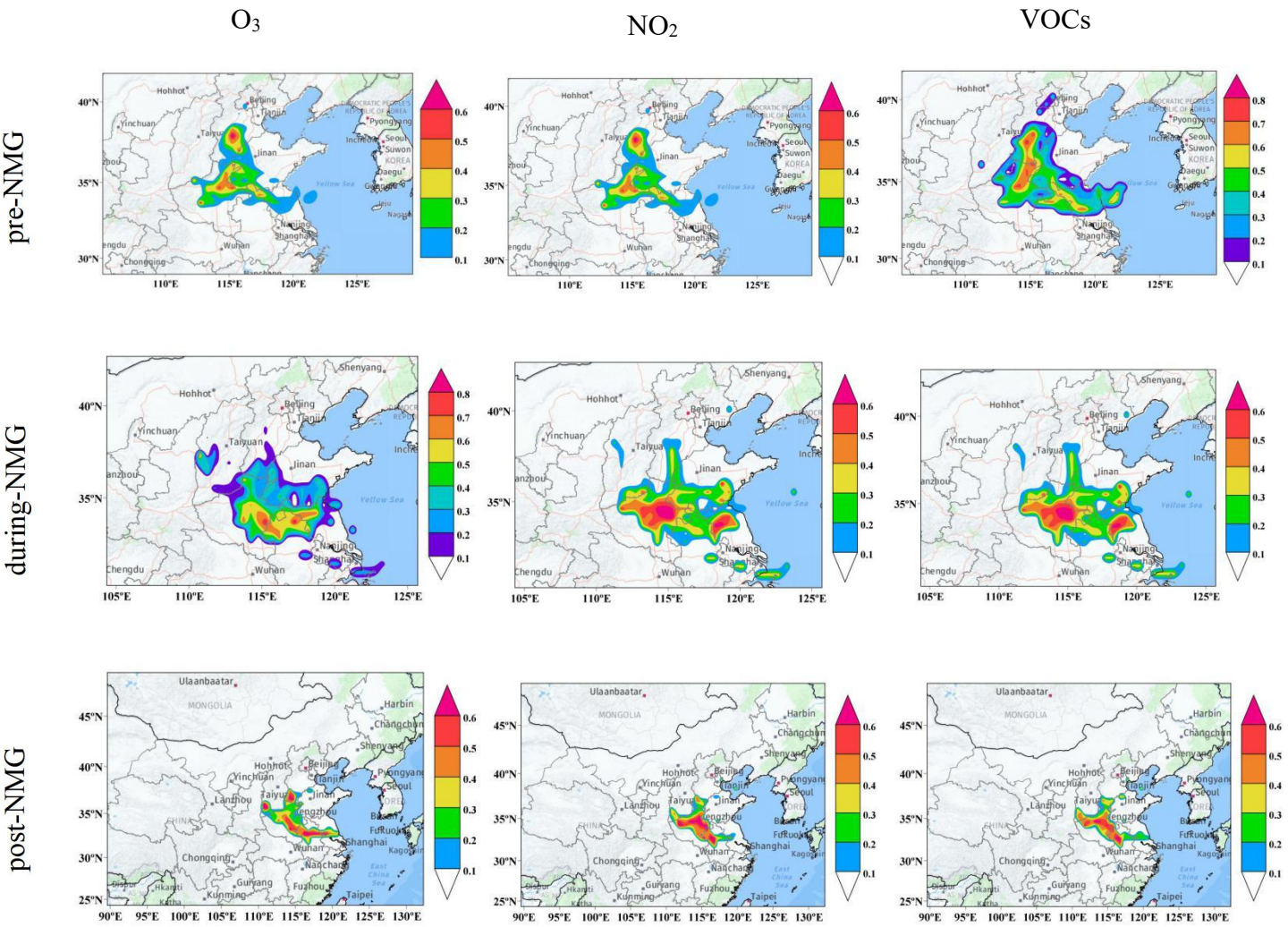

Fig. 2 The average weighted PSCF maps for O_3, NO_2 and VOCs in Zhengzhou during the three periods.

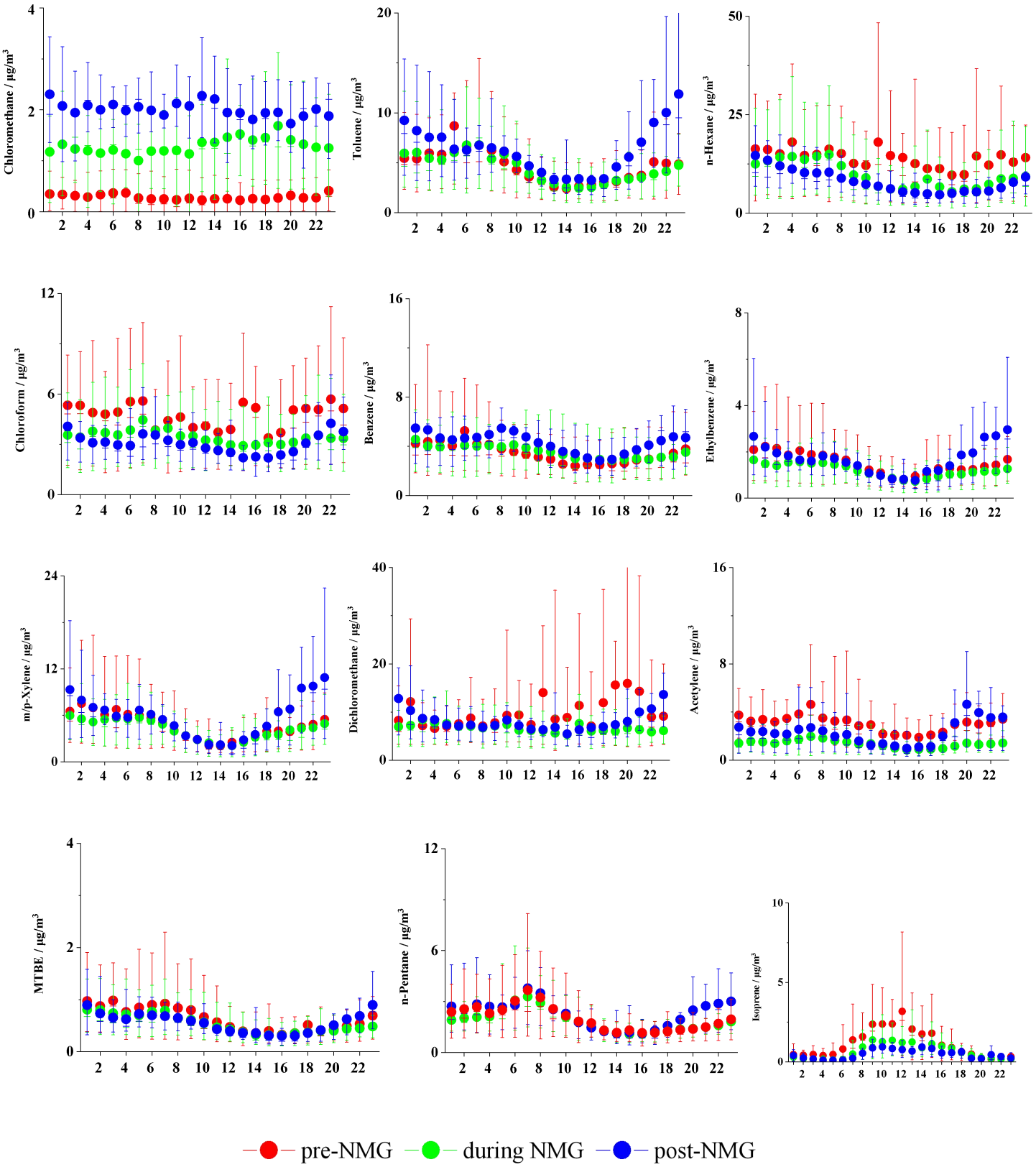

Fig. 3 Diurnal variations in concentrations of some reactive VOC species in Zhengzhou during the three periods.

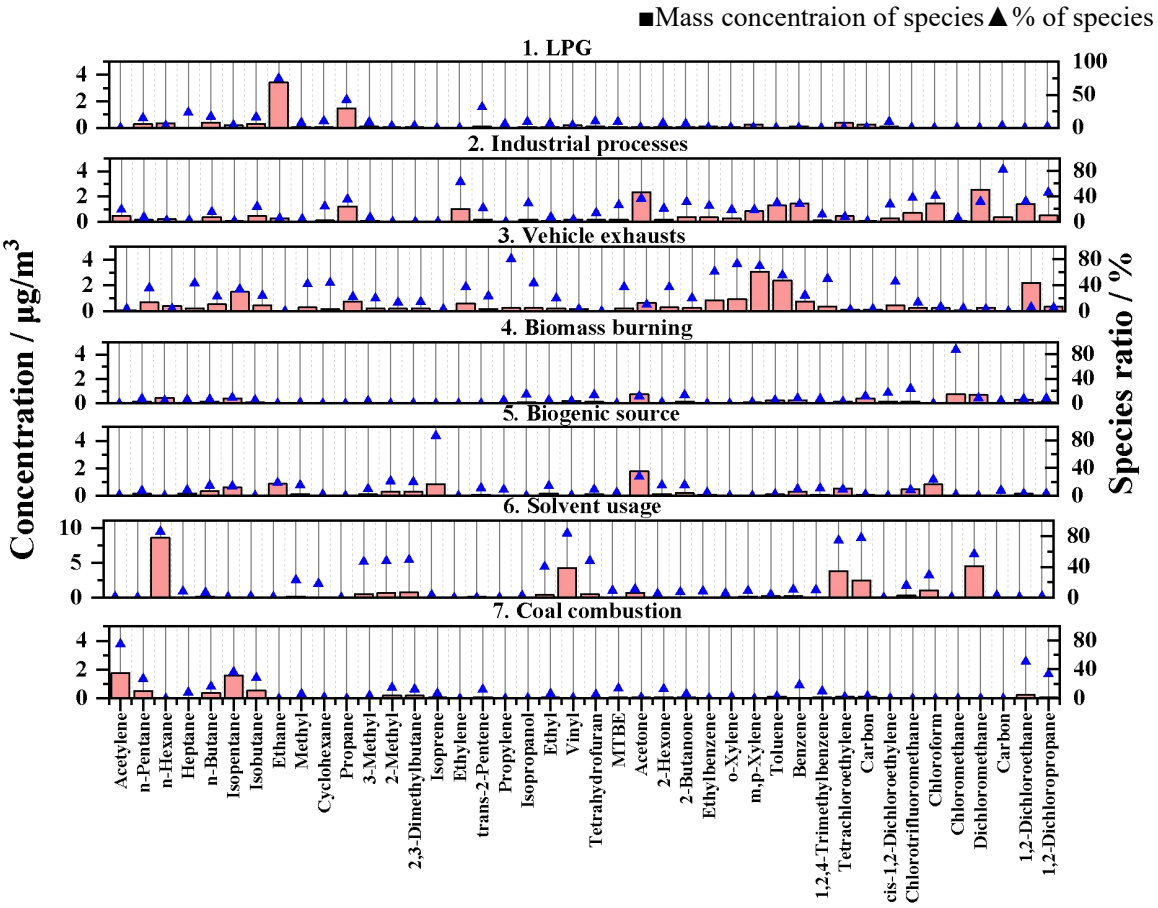

Fig. 4 Source profiles calculated using the PMF model.

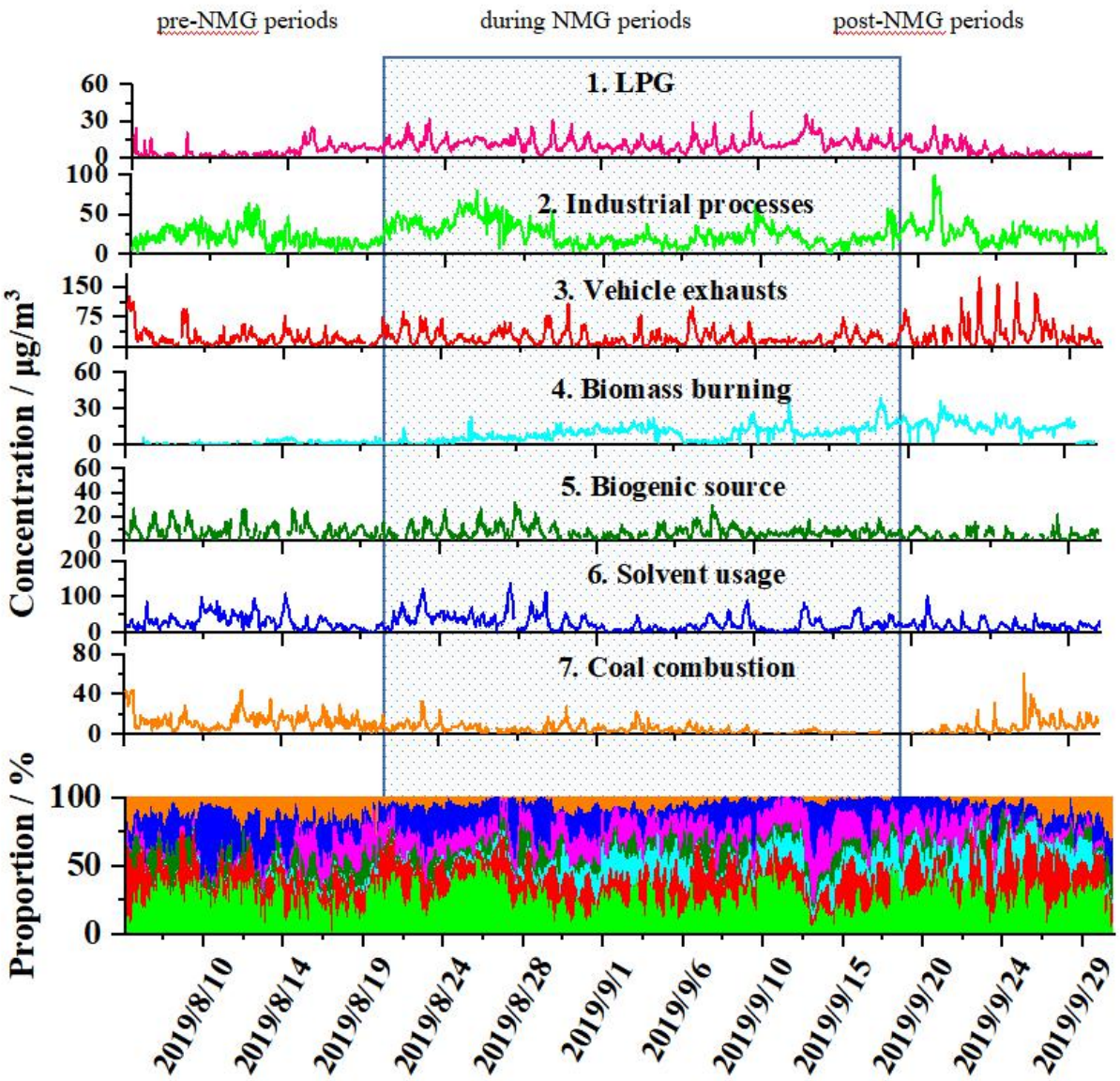

Fig. 5 Time series of each identified source contributions and accumulated relative VOC contributions.

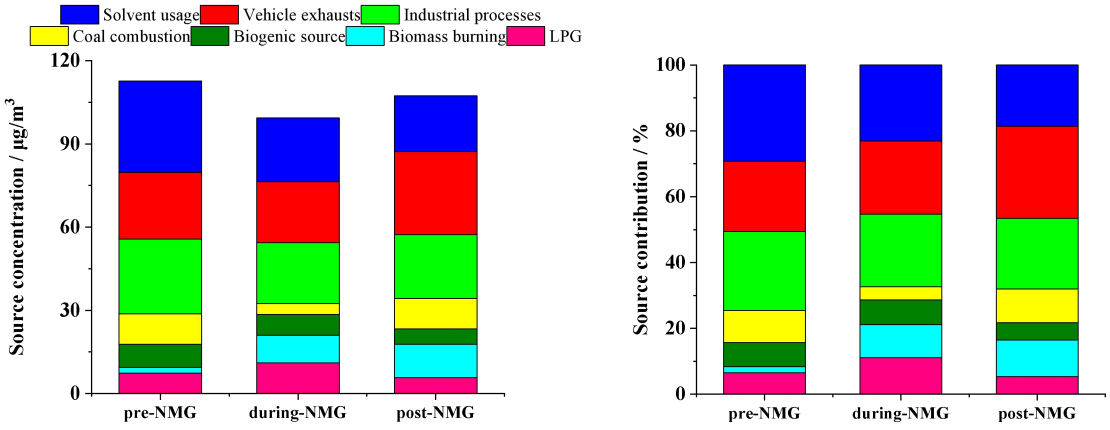

Fig. 6 Source contributions to VOCs concentration in the PMF model during the three period.

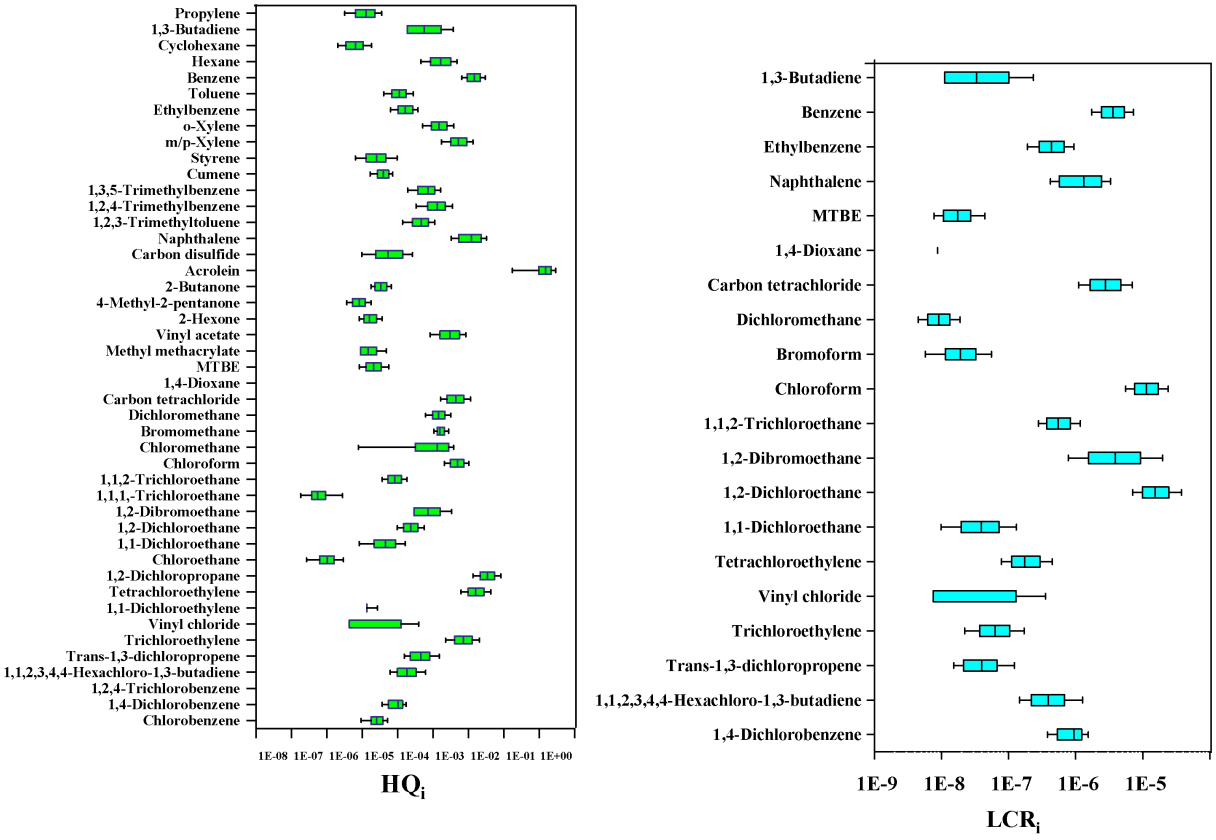

Fig. 7 Non-carcinogenic risks of HQ and carcinogenic risks for individual VOC species.

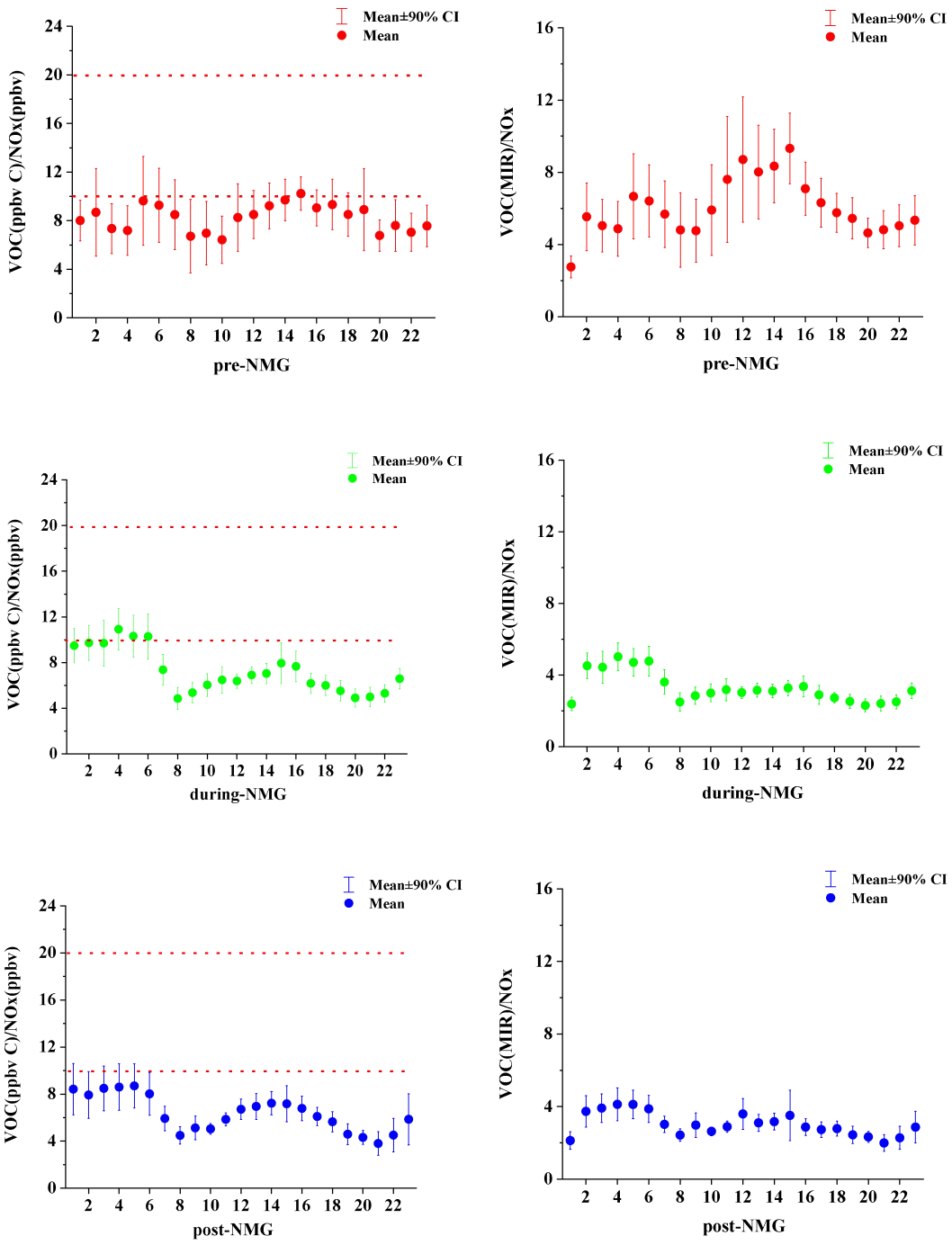

Fig. 8 Daily variations in the VOC/NOx ratio in Zhengzhou before, during, and after NMG periods.

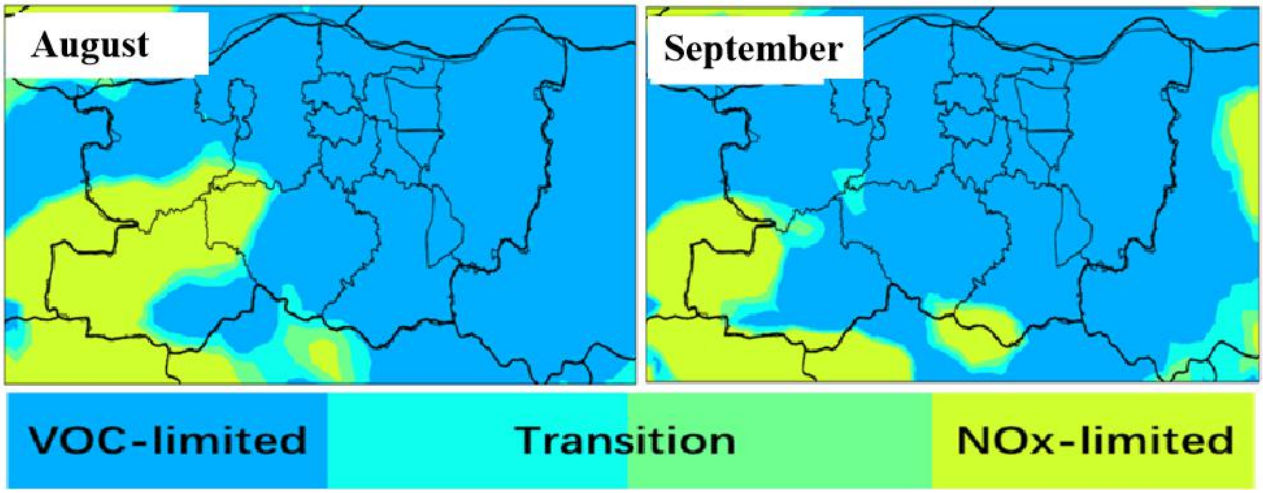

Fig. 9 Spatial comparison of O_3-NOx-VOCs sensitive regime between August and September 2019 in Zhengzhou.

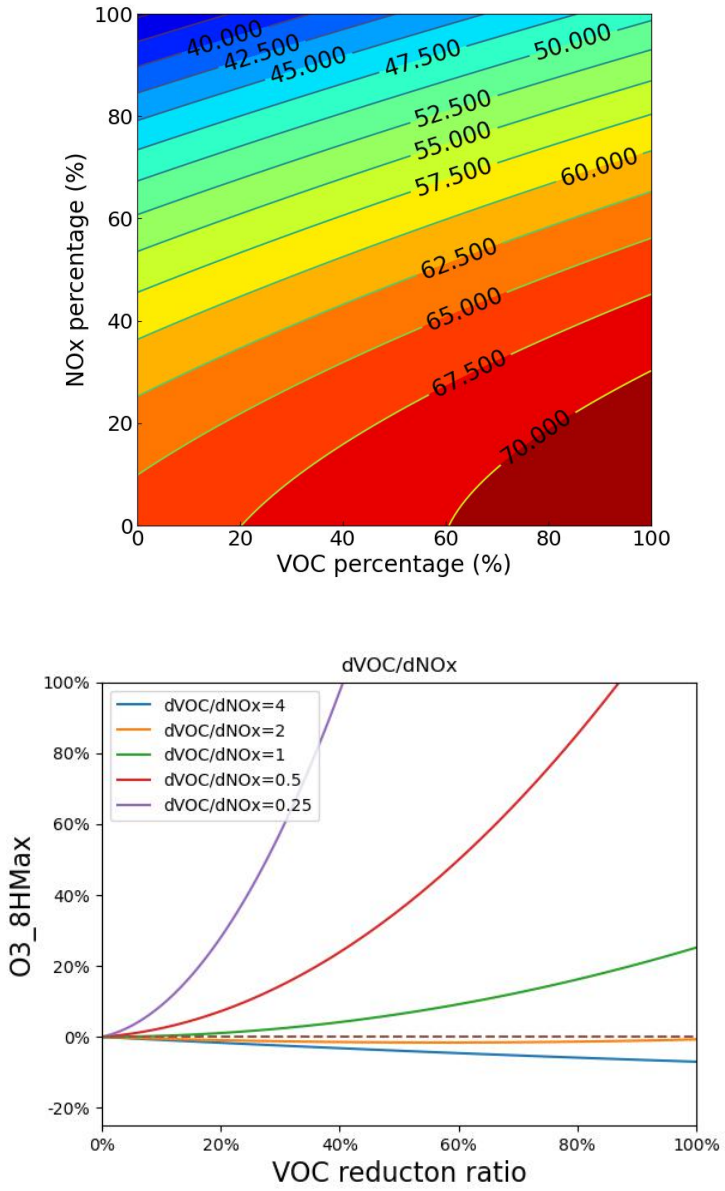

Fig. 10 The O_3 isopleth diagram versus NOX and VOCs using EKMA (a) and variation chart of O_3 concentration in each control path (b) during pre-NMG period in Zhengzhou.

Table list

Table 1 Concentrations of the 20 most abundant species in Zhengzhou (unit: μg/m^3).

Component	Before	Component	During	Component	After
n-Hexane	16.5	n-Hexane	9.6	Dichloromethane	8.1
Dichloromethane	12.6	Dichloromethane	6.7	n-Hexane	8.1
Vinyl acetate	8.4	Acetone	6.5	Acetone	7
Acetone	7.6	Ethane	5.7	Toluene	6.3
Tetrachloroethylene	6.6	Tetrachloroethylene	5.3	1,2-Dichloroethane	6.1
1,2-Dichloroethane	5	Vinyl acetate	4.9	m,p-Xylene	5.8
Toluene	4.9	1,2-Dichloroethane	4.6	Propane	5.1
Chloroform	4.8	Toluene	4.5	Isopentane	5
m,p-Xylene	4.7	m,p-Xylene	4.3	Benzene	4.3
Isopentane	4.6	Propane	4.2	Ethane	4.3
Ethane	4.2	Carbon tetrachloride	4.1	Tetrachloroethylene	4.1
Carbon tetrachloride	3.9	Isopentane	3.7	Vinyl acetate	4
Propane	3.8	Benzene	3.6	Carbon tetrachloride	3.6
Benzene	3.6	Chloroform	3.5	Chloroform	3.1
Acetylene	3.1	n-Butane	2.1	Acetylene	2.9
n-Butane	2.5	Freon 11	2	n-Butane	2.8
Isobutane	2.2	Isobutane	1.9	Isobutane	2.5
Freon 11	2	n-Pentane	1.9	Ethylene	2.5
n-Pentane	2	Ethylene	1.7	n-Pentane	2.5
Ethylbenzene	1.5	Acetylene	1.4	Methyl chloride	1.9
∑TOP 20 species	104.5		82.2		90.0
∑TOP 20 species / ∑ VOCs	70%		68%		66%

Table 2 OFP contributions (μg/m^3) of each VOC source during the sampling periods in Zhengzhou.

Source	Source contribution		
	pre-NMG	during-NMG	post-NMG
LPG	8.7	13	6.9
biomass burning	1.5	8.4	9.8
Biogenic source	18.6	16.6	13.1
coal combustion	14.6	4.8	14.9
industrial processes	41.4	33.3	35.5
vehicle exhausts	72.1	65.3	89
Solvent use	46.2	32.1	28.8
Totol	203.1	173.5	198.0